

NASA Technical Memorandum 4536

Simultaneous Solution for Core Magnetic Field and Fluid Flow Beneath an Electrically Conducting Mantle

Coerte V. Voorhies
*Goddard Space Flight Center
Greenbelt, Maryland*

Masahiro Nishihama
*Hughes STX Corporation
Lanham, Maryland*



National Aeronautics and
Space Administration

Goddard Space Flight Center
Greenbelt, Maryland 20771



Simultaneous Solution for Core Magnetic Field and Fluid Flow Beneath an Electrically Conducting Mantle

Coerte V. Voorhies
Geodynamics Branch, Code 921/NASA,
Goddard Space Flight Center Greenbelt, MD 20771
Masahiro Nishihama
Hughes STX Corp., Lanham, MD 20706
Submitted to the
Journal of Geophysical Research
August 17, 1993

Abstract. The effects of laterally homogeneous mantle electrical conductivity have been included in steady, frozen-flux core surface flow estimation along with refinements in method and weighting. The refined method allows simultaneous solution for both the initial radial geomagnetic field component at the core-mantle boundary (CMB) and the sub-adjacent fluid motion; it also features Gauss' method for solving the non-linear inverse problem associated with steady motional induction. The tradeoff between spatial complexity of the derived flows and misfit to the weighted Definitive Geomagnetic Reference Field models (DGRFs) is studied for various mantle conductivity profiles. For simple flow and a fixed initial geomagnetic condition, a fairly high deep-mantle conductivity performs better than either insulating or weakly conducting profiles; however, a thin, very high conductivity layer at the base of the mantle performs almost as well. Simultaneous solution for both initial geomagnetic field and fluid flow reduces the misfit per degree of freedom even more than does changing the mantle conductivity profile. Moreover, when both core field and flow are estimated, the performance of the solutions and the derived flows become insensitive to the conductivity profile.

Introduction

Perhaps the simplest magnetic Earth model is the source-free mantle/frozen-flux core model, wherein an effectively rigid, impenetrable, electrically insulating mantle of uniform magnetic permeability surrounds an effectively spherical, inviscid, perfectly conducting liquid outer core in anelastic flow. This basic Earth model indicates vacuum extrapolation of broad-scale potential geomagnetic field models to the CMB and attributes geomagnetic secular variation (SV) to advection of the footpoints of geomagnetic force field lines by the fluid motion at the top of the core. This process is described in terms of the radial component of the frozen-flux induction equation at the top of the core:

$$\partial_t B_r + \nabla_s \cdot B_r v = 0 \quad (1)$$

where B_r is the radial component of the magnetic flux density vector, v is the fluid velocity vector, and $\nabla_s \cdot$ is the surface divergence operator [see, e.g., Roberts & Scott, 1965; Backus, 1968; Voorhies, 1986a, 1991].

This magnetic Earth model has been widely tested and has proven to be quite useful. For example, the CMB was located geomagnetically [Hide & Malin, 1981; Voorhies & Benton, 1982] and contour maps of the broad-scale radial geomagnetic field component near the CMB were constructed and analyzed over a decade ago using this model [Booker, 1969; Benton *et al.*, 1979; Voorhies, 1984; Bloxham & Jackson, 1992]. Steady fluid flows near the top of the core have been estimated geomagnetically—both with and without the surficially geostrophic flow constraint—using this model (see, e.g., Voorhies & Backus [1985]; Backus & LeMouél [1986]; reviews by Voorhies [1987] and Bloxham & Jackson [1991]; and more recent work by Bloxham [1992]; Davis & Whaler [1993]; Voorhies [1991, 1993]; and Whaler [1991]). Contour plots of millibar pressure perturbations at the core surface have been derived from steady, tangentially geostrophic core flow estimates [Voorhies, 1991]. Steady and piecewise steady flow estimation procedures

have been improved during the past decade—in part because Earth rotation data suggest that fluctuations in near-surface core flow are small (about 1 km/yr) [Voorhies, 1993; but also see Benton & Celaya, 1991 and Jackson *et al.*, 1993].

Motivation

The source-free mantle/frozen-flux core model previously used to locate the core and estimate its near-surface flow is a seemingly sound first approximation. The significance of evidence suggesting magnetic flux diffusion at the CMB may be debated despite the finite electrical conductivity of liquid iron alloys [see, e.g., Booker, 1969; Voorhies, 1984, 1986a; Bloxham & Gubbins, 1986; Benton & Voorhies, 1987; Bloxham & Jackson, 1992; Constable *et al.*, 1993]. Nevertheless, this simple Earth model is but an idealization which is not sustained by mineral physics data. Elimination of the frozen-flux core approximation in favor of steady magnetic flux diffusion led to steady diffusive flows which provide a closer fit to the weighted DGRFs [IAGA, 1988] than do steady frozen-flux flows; moreover, the negative correlation found between advective and diffusive contributions to core SV substantiates the core geodynamo hypothesis [Voorhies, 1993]. It was also found that laterally heterogeneous steady flux diffusion need not appreciably alter steady surficial core flow estimates; therefore, geomagnetic effects of lateral heterogeneity in deep-mantle conductivity are arguably small.

Much as Earth's core is not a perfect conductor, Earth's mantle is not a perfect resistor; therefore, one should correct core surface field and flow estimates for the effects of mantle conductivity. These corrections are not easily made because there is little agreement as to the value of mantle conductivity—even as a spherically averaged function of radius alone, $\sigma_m(r)$. Figure 1 portrays six mantle conductivity profiles; the logarithmic ordinate highlights the relatively poor agreement among authors. It seems that more recent experiments measuring the conductivity of ferro-magnesian silicates at high pressure do not settle the mantle conductivity problem due to the uncertain composition and temperature of the deep mantle [Li & Jeanloz, 1987; Peyronneau & Poirier, 1989]. In this situation, one can but try various profiles and see which, if any, are more consistent with the data and models underlying core field and flow estimation.

Effects of Mantle Conductivity

The qualitative geomagnetic effects of a laterally homogeneous mantle conductivity can be deduced by examining solutions to the classic problem of magnetic diffusion through a sphere of radially varying conductivity [Lahiri & Price, 1939; McDonald, 1957; Benton & Whaler, 1982; Backus, 1982, 1983]. For magnetic flux density vector \mathbf{B} , electrical conductivity σ_m , and uniform magnetic permeability μ , the laws of Faraday, Ohm, and Ampere yield

$$\partial_t \mathbf{B} = (\mu \sigma_m)^{-1} [\nabla^2 \mathbf{B} + \nabla(\ln \sigma_m) \times \nabla \times \mathbf{B}] \quad (2)$$

For laterally homogeneous $\sigma_m(r)$ in spherical polar coordinates (r, θ, ϕ) , the radial diffusion equation is just

$$\partial_t B_r = (\mu \sigma_m r)^{-1} \nabla_r^2 B_r \quad (3)$$

Alternatively, one may consider the Mie representation of the solenoidal geomagnetic flux density, $\mathbf{B} = \nabla \times [\mathbf{r} \times \nabla P] + \mathbf{r} \times \nabla Q$, where P and Q are, respectively, the poloidal and toroidal scalars which average to zero on spheres and $B_r = -r \nabla_s^2 P$ for surface Laplacian ∇_s^2 [Backus, 1986]; then P and Q decouple in equation (2) and the diffusion equation for the poloidal scalar is $\partial_t P = [\mu \sigma_m]^{-1} \nabla^2 P$.

Because the deep mantle is of primary concern, we consider a single power-law profile, $\sigma_m = \sigma_0 (r/c)^{-\lambda}$ with core radius $c = 3480$ km. Then equation (3) has solutions separable into spherical

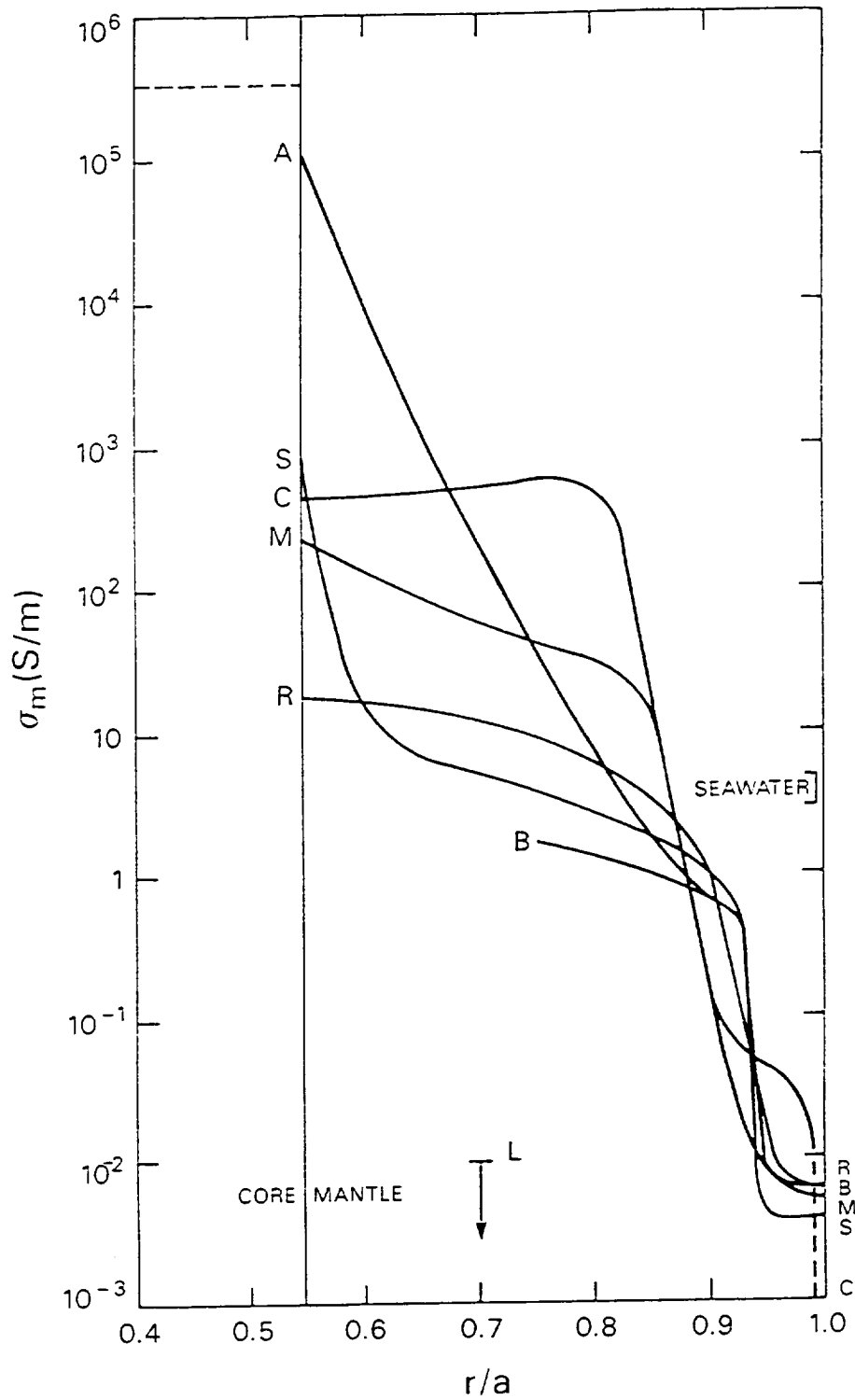


Fig. 1. Electrical conductivity of the mantle, σ_m , in S/m as a function of normalized Earth radius, r/a , according to various authors: profile M—*McDonald* [1957], B—*Banks* [1969], C—*Eckhardt et al.* [1963], R—*Rikitake* [1973], A—*Aldredge* [1977], S—*Stacey* [1977], L—*Li & Jeanloz* [1987] upper limit. Also shown are the conductivity of seawater and a plausible core conductivity (dashed line at 3×10^5 S/m).

harmonics, Fourier series in time, and Bessel functions of imaginary argument and irrational order in radius [McDonald, 1957]. In particular, we introduce the compact spherical harmonic expansions for B_r near Earth's surface ($r = a = 6371.2$ km) and near the CMB ($r = c$):

$$B_r(a, \theta, \phi; t) = \sum_i \gamma_i(t) S_i(\theta, \phi) \quad (4a)$$

$$B_r(c, \theta, \phi; t) = \sum_i \Gamma_i(t) S_i(\theta, \phi) \quad (4b)$$

The S_i notation is that of Voorhies [1986b]: let P_n^m represent the Schmidt normalized associated Legendre polynomial of degree n and order m ; then for $i = n^2$ and $m = 0$, $S_i = P_n^0(\cos\theta)$, and for $i = n^2 + 2m - 1$ and $m \neq 0$, $S_i = P_n^m(\cos\theta)\cos m\phi$ and $S_{i+1} = P_n^m(\cos\theta)\sin m\phi$. If each spherical harmonic coefficient at the CMB is expressed as the sum of a baseline linear temporal trend and real temporal oscillations,

$$\Gamma_k(t) = \Gamma_k^0 + \Gamma_k^1 [t - t_0] + \frac{1}{2} \sum_l [\Gamma_k^l e^{i\omega_l(t-t_0)} + \Gamma_k^{l*} e^{-i\omega_l(t-t_0)}] \quad (5)$$

then the spherical harmonic coefficient near Earth's surface is the geometric upward continuation of the delayed baseline and the phase-lagged, physically attenuated oscillations:

$$\gamma_k(t) = \left(\frac{c}{a}\right)^{n_k+2} \left\{ \Gamma_k^0 + \Gamma_k^1 [t - t_0] - \frac{\mu\sigma_0 c^2}{(\lambda-2)(\lambda+2n_k-1)} \left(1 - \left(\frac{c}{a}\right)^{\lambda-2}\right) \right\} + \frac{1}{2} \sum_l \left[\Gamma_k^l \frac{f_k^l(a)^* f_k^l(c)}{f_k^l(c)^* f_k^l(c)} e^{i\omega_l(t-t_0)} + \Gamma_k^{l*} \frac{f_k^l(c)^* f_k^l(a)}{f_k^l(c)^* f_k^l(c)} e^{-i\omega_l(t-t_0)} \right] \quad (6a)$$

where

$$f_k^l(r) = \sum_{j=0}^{\infty} \frac{(i)^j}{j!} \left[\frac{\omega_l \mu \sigma_0 c^2}{(\lambda-2)^2} \left(\frac{r}{c}\right)^{2-\lambda-j} \right] / \Gamma(v_k + j + 1) \quad (6b)$$

$\Gamma(v_k + j + 1)$ is the gamma function, $v_k = (2n_k + 1)/(\lambda - 2)$, and n_k is the spherical harmonic degree of the k^{th} coefficient. More generally, we can introduce temporal basis functions $T^l(t)$, the temporal coefficients Γ_k^m of $\Gamma_k(t)$, and the upward continuation operator Υ_{pk}^{lm} :

$$\gamma_p(t) = \sum_l \sum_k \sum_m T^l(t) \Upsilon_{pk}^{lm} \Gamma_k^m \quad (7)$$

By Lenz's law, a change in the core field induces electric currents in the mantle which oppose the change. So SV must fight its way through the mantle. The greater the mantle conductivity, the longer the fight and the greater the losses. Fourier analysis of the diffusion equation for the spherical harmonic coefficients of the radial geomagnetic field component reveals that the mantle filter is dispersive: at each harmonic degree, different frequencies diffuse across the mantle with different time lags. This implies a loss of the simultaneity enjoyed by source-free mantle treatments of the core field. Moreover, the physical attenuation of a signal diffusing through the mantle suggests that more vigorous SV at the CMB will be needed to match the observed SV than is needed in the insulating mantle case. More vigorous SV at the CMB suggests more vigorous core surface flow, so one expects a more vigorous core flow estimate when mantle conductivity is included.

Method

Our numerical method for estimating the core field and flow just beneath a conducting mantle is designed for a damped weighted least-squares fit to the DGRFs [IAGA, 1988] for the 35-year interval between 1945 and 1980. The cost function minimized is the sum of the square-weighted residual relative to the eight DGRFs spanning this interval at 5-year epochs plus the damped mean square swirl and mean square confluence of the fluid flow at the top of the core. Denote by $g_p(t_s)$ the p^{th} DGRF radial field coefficient ($p \leq 120$) at time $t_s = 1940 + 5s$ ($1 \leq s \leq 8$); then this cost function is $\Delta^2 = \Delta_r^2 + \lambda_d \Delta_d^2$ or

$$\Delta^2 = \sum_{s=1}^8 \sum_{p=1}^{120} \sum_{q=1}^{120} [g_p(t_s) - \gamma_p(t_s)] W_{pq}(t_s) [g_q(t_s) - \gamma_q(t_s)] \quad (8)$$

$$+ \frac{\lambda_d}{4\pi} \int_0^{2\pi} \int_0^{\pi} [\omega_r^2 + (\partial_r u)^2] \sin\theta d\theta d\phi$$

where $W_{pq}(t_s)$ is the weight matrix for epoch t_s , λ_d is the damping parameter, and $\omega_r \equiv \hat{r} \cdot \nabla \times \mathbf{v}$ is the radial vorticity (swirl) and $\partial_r u = -\nabla_s \cdot \mathbf{v}$ is the surface convergence (confluence) of the surficial fluid velocity.

Following Voorhies [1986b], steady $\mathbf{v}(c, \theta, \phi) = v\hat{\theta} + w\hat{\phi}$ is expressed in terms of the spherical harmonic expansions for its streamfunction and velocity potential: $\mathbf{v} = \hat{r} \times \nabla_s(\sum_j \alpha_j S_j) + \nabla_s(\sum_j \beta_j S_j)$. Then with (4b), (1) becomes

$$\partial_t \Gamma_k(t) = \sum_i \sum_j \Gamma_i(t) [X_{ijk} \alpha_j + Y_{ijk} \beta_j] \quad (9a)$$

$$= \sum_j [P_{kj}(t) \alpha_j + Q_{kj}(t) \beta_j] \quad (9b)$$

$$= \sum_i Z_{ki} \Gamma_i(t) \quad (9c)$$

where, after integration by parts over the CMB,

$$P_{kj} = \frac{2n_k+1}{4\pi c^2} \int_0^{2\pi} \int_0^{\pi} B_r [\partial_\phi S_j \partial_\theta S_k - \partial_\theta S_j \partial_\phi S_k] d\theta d\phi \quad (10a)$$

$$Q_{kj} = \frac{2n_k+1}{4\pi c^2} \int_0^{2\pi} \int_0^{\pi} B_r [\partial_\theta S_j \partial_\theta S_k + \partial_\phi S_j \partial_\phi S_k / \sin^2 \theta] \sin\theta d\theta d\phi \quad (10b)$$

and

$$Z_{ki} = \frac{2n_k+1}{4\pi c^2} \int_0^{2\pi} \int_0^{\pi} [S_i \partial_r u - \partial_\theta S_i v - \partial_\phi S_i w / \sin\theta] S_k \sin\theta d\theta d\phi \quad (10c)$$

Note that the solution of (9c) is of propagator form

$$\Gamma(t) = \{\exp[(t - t_0)Z]\} \Gamma(t_0) = \wp(t) \Gamma(t_0) \quad (11)$$

where Γ is the vector of elements Γ_k , Z is the matrix of elements Z_{ki} , and \wp is the propagator matrix. Truncation of Z to an $N \times N$ square matrix and eigen-decomposition thereof yields the complex eigenvalues

which are the growth/decay rates and frequencies of oscillation of elemental magnetic modes; unfortunately, the number and magnitude of these eigenvalues depends upon the chosen value of N .

To implement the Gauss method for solving the nonlinear geophysical inverse problem posed by the minimization of (8) with respect to the model parameters $(\alpha, \beta, \Gamma(t_0))$, one needs the coefficients of the normal equations matrix A at each iteration. To linearize and iterate, set

$$\delta\gamma_p(t) = \sum_q \left[\frac{\partial\gamma_p(t)}{\partial\Gamma_q(t_0)} \delta\Gamma_q(t_0) + \frac{\partial\gamma_p(t)}{\partial\alpha_q} \delta\alpha_q + \frac{\partial\gamma_p(t)}{\partial\beta_q} \delta\beta_q \right] = \sum_j A_{pj}(t) \delta\xi_j \quad (12)$$

recall the temporal basis functions $T^n(t)$, and introduce the orthonormalization matrix $L = M^{-1}$ where

$$M^{nm} = \int_{t^-}^{t^+} T^n(t) T^m(t) dt$$

and (t^-, t^+) are the limits of integration: $t^- \leq t_0 \leq t^+$. Then

$$\gamma_p(t) = \sum_l \sum_k \sum_m \sum_n T^l(t) Y_{pk} \text{Im} L^{mn} \int_{t^-}^{t^+} \Gamma_k(t) T^n(t) dt \quad (13)$$

and the partial derivatives in (12) are just the reassembled upward continuation of the transformed $\partial\Gamma_k(t)/\partial\Gamma_q(t_0)$, $\partial\Gamma_k(t)/\partial\alpha_q$, and $\partial\Gamma_k(t)/\partial\beta_q$. Clearly

$$\frac{\partial\Gamma_k(t)}{\partial\Gamma_q(t_0)} = \{ e^{(t-t_0)Z} \}_{kq} = I_{kq} + Z_{kq}(t-t_0) + \sum_a Z_{ka} Z_{aq} \frac{(t-t_0)^2}{2} + \dots \quad (14a)$$

while, after some manipulation involving the inverse of the propagator [Sabaka *et al.*, 1992], it can be shown that

$$\frac{\partial\Gamma_k(t)}{\partial\alpha_q} = \int_{t_0}^t \sum_v \{ e^{(t-\tau)Z} \}_{kv} P_{vq}(\tau) d\tau \quad (14b)$$

$$\frac{\partial\Gamma_k(t)}{\partial\beta_q} = \int_{t_0}^t \sum_v \{ e^{(t-\tau)Z} \}_{kv} Q_{vq}(\tau) d\tau \quad (14c)$$

Substitution of (14) into the partial derivatives of (13) with respect to the model parameters gives the elements of the normal equations matrix A_{pj} appearing in (12).

Application

In practice, the calculations have three phases: (a) initial A matrix element generation; (b) first flow and second A matrix element generation; and (c) iteration. In phase (a), a baseline trend and a Fourier sine series are fitted exactly through the sequence of input DGRF radial field coefficients [Allredge, 1987].

These coefficients are downwardly continued to the CMB, noting that the baseline field leads at the CMB and the Fourier series enjoys the usual phase lead and physical amplification at the CMB (see 6a). Initial P_{kj} and Q_{kj} are computed at 5-year intervals by numerical integration of (10a-b) and used to evaluate (14) numerically with $Z = 0$. The upward continuation indicated by the partial derivatives of (13) is achieved via discrete Fourier cosine transform (DFCT) over the doubled time interval [$t_- = 1930, t_+ = 2000$]; then the A matrix elements are reassembled at the 8 DGRF epochs using the attenuated, phase-shifted cosinusoids.

In phase (b), the weighted information matrix (A^TWA) is assembled and damped. The first flow estimate (complete through degree and order 13) is obtained by the usual damped weighted least-squares estimator. This flow field is used to solve the forward steady motional induction problem (1) numerically. We start at epoch $t_0 = 1965$, advect forward to 2000, and then restart at 1965 and advect back to 1930. Γ , P , and Q are evaluated annually with a high-accuracy numerical quadrature on a $1^0 \times 2^0$ mesh (the pole corrections actually yield fifth order-accuracy or better). We use a DFCT of Γ over the doubled, 70-year interval (Nyquist period of 2 years). This procedure is in accord with changing the sign of the fluid velocity every 70 years; it generates a purely periodic prediction for B_T and rolls back edge effects away from the target interval 1945-1980. We then upwardly continue the coefficients of the predicted field at the CMB through the conducting mantle, evaluate $\gamma_p(t_s)$, and calculate the residuals relative to the DGRFs. The flow is used to evaluate Z (truncated to 224×224); the truncated propagator in (14) is represented by the cubic polynomial—a fair approximation for the slow flows over short intervals studied. We then compute the DFCT of the propagated P and Q matrices (without recourse to the matrix convolution theorem). The DFCTs of propagated P and Q are then upwardly continued and used to evaluate second A matrix elements at the DGRF epochs.

In phase (c), the new information matrix is assembled, damped, and used to estimate the second flow. This in turn allows calculation of the second prediction; Γ ; residuals ($g_p(t_s) - \gamma_p(t_s)$); P , Q , and Z ; the propagator $\phi(t)$; and a third set of A matrix elements. Iteration is continued until the velocity field changes by less than 1%. Note that it is only on the second and higher iterations that we have the estimate of α and β needed to evaluate Z —and thus meaningfully estimate the initial condition, $\Gamma(t_0)$. When this option is exercised, the $\Gamma_k(t_0)$ are estimated through degree and order 10.

The weights employed differ somewhat from those used by Voorhies [1993]. The improved covariance matrix for the 1980 DGRF is from Langel *et al.* [1989]. Because this parameter covariance was derived using an approximate correlated data weight matrix, it overestimates parameter uncertainty. The results shown in Table 10 of Langel *et al.* [1989] were thus used to reduce this 1980 covariance matrix—thereby increasing the weight matrix elements. The resulting weight matrix still appeared too light compared with weight matrices derived for epochs 1965, 1970, and 1975 from the DGRF candidate models. To achieve a satisfactory temporal distribution of weights, the 1965-1975 weight matrices were multiplied by 2/3 and the 1980 weight matrix was multiplied by 2.40—the exact factor being chosen to preserve the cumulative weighted variance in the DGRF models relative to 1965.

Results

We chose four mantle conductivity profiles to study in some detail. Profile A is just the insulating mantle case ($\sigma_m = 0$). For profile C the conductivity at the base of the mantle is 300 S/m; for profile E it is 3,000 S/m. Both profiles C and E have a conductivity of 1 S/m at 0.9a; therefore, profile C is $\sigma_m = 300(c/r)^{11.42}$ and profile E is $\sigma_m = 3,000(c/r)^{16.03}$. For profile G the conductivity is 10^5 S/m at the base of the mantle and falls off to 1 S/m 200 km above the CMB; therefore, profile G is $\sigma_m = 10^5(c/r)^{123.6}$. For the deep mantle, conductivity profile C is similar to the profiles favored by Achache *et al.* [1981]. Profile E represents a fairly high deep-mantle conductivity. Profile G corresponds to a thin, highly conducting layer just above the core—such as might result from the combined effects of wüstite overplating of the core and deep-mantle convection (wüstite being metallic at high pressures and temperatures according to Knittle *et al.* [1986]).

Fixed Initial Conditions

For each of the four mantle conductivity profiles studied, we solved the steady surficial core flow estimation problem at various λ_d so as to develop a trade-off curve of "flow complexity" as a function of "misfit". The flow complexity is the square root of the mean square swirl plus the mean square confluence of the flow, Δ_d . The misfit is the square root of the square weighted residual per degree of freedom, $(\Delta_T^2/\text{DOF})^{1/2}$. The number of degrees of freedom of the solution (DOF) is taken to be 840 minus the trace of the resolution matrix: the number of $\gamma_p(t_s)$ fitted minus the 120 coefficients of the fixed initial geomagnetic condition equals 840; the trace of the resolution matrix was less than 90.21 in all cases studied. The latter shows that damping, rather than truncation of the streamfunction and velocity potential expansions to degree 13, dominates the regularization. The weight matrices for the DGRFs are uncertain; however, the measure of misfit is thought to be within a factor of 2 of the square root of chi-squared per degree of freedom—with our misfit likely exceeding $(\chi^2/\text{DOF})^{1/2}$.

These four trade-off curves are plotted in Figure 2. The minimum misfit achieved was 6.53, was for a flow complexity of $1.04 \times 10^{-2} \text{ yr}^{-1}$, and was at the modest RMS flow speed of 8.98 km/yr. The curves differ but slightly despite the large changes in the mantle conductivity adopted; moreover, inspection of vector plots of solutions around the knees of the tradeoff curves shows these flow fields to be visually indistinguishable. Above the knees of the trade-off curves, there is evidence confirming that more vigorous flow is needed to achieve a given misfit when the effects of mantle conductivity are included in steady surficial core flow estimation. At and below the knee of the trade-off curves, conductivity profile E clearly out-performs the other profiles studied: in this region, profile E gives lower misfit at fixed flow complexity than do the other profiles. Still, profile G performs only slightly worse than profile E. The inference that profile E is more compatible with the attribution of definitive secular change to steady surficial frozen-flux core flow is, however, unwarranted: further work shows such an inference to be an artifact of holding the initial geomagnetic condition fixed.

Simultaneous Solutions for Core Field and Flow

Figure 3 shows the trade-off curves of flow complexity as a function of misfit in the case of an insulating mantle from the fixed initial condition flows (solid curve) and from simultaneous solutions for both the initial core field and the steady core surface flow (dot-dashed curve). The misfit is still $(\Delta_T^2/\text{DOF})^{1/2}$, but DOF is now 960 minus the trace of the resolution matrix. Simultaneous estimation of both core field and flow clearly out-performs estimation of the flow alone: at any level of flow complexity studied, the simultaneous solutions offer substantially reduced square-weighted residuals *per degree of freedom* when compared with the solutions for the flow alone. The minimum misfit achieved was 5.20, was for a flow complexity of $8.11 \times 10^{-3} \text{ yr}^{-1}$, was at an RMS flow speed of 8.44 km/yr, and was for 193.1 effectively free parameters (120 being for the initial core field). Again, the misfit is thought to overestimate $(\chi^2/\text{DOF})^{1/2}$ by a factor of up to 2.

The difference between the two curves plotted in Figure 3 confirms the importance of initial conditions in determining the quality of the solution. As evidenced by equation (11), the difference between fields predicted by the action of a steady flow on slightly different initial magnetic conditions can grow exponentially in time [Voorhies, 1992].

Simultaneous solutions for core field and flow at various λ_d were also derived for mantle conductivity profiles E and G. These tradeoff curves are visually indistinguishable from the insulating mantle (dot-dashed) curve in Figure 3. The effects of laterally homogeneous mantle conductivity on the performance of steady surficial core flow solutions are thus negligible provided both the initial radial geomagnetic component and the core flow at the CMB are estimated. It follows that all conductivity profiles in the range studied are equally compatible (or equally incompatible) with the attribution of definitive secular geomagnetic change to steady surficial frozen-flux core flow. Moreover, vector plots of the flows derived for different profiles (but at the same λ_d) are visually indistinguishable. This implies that

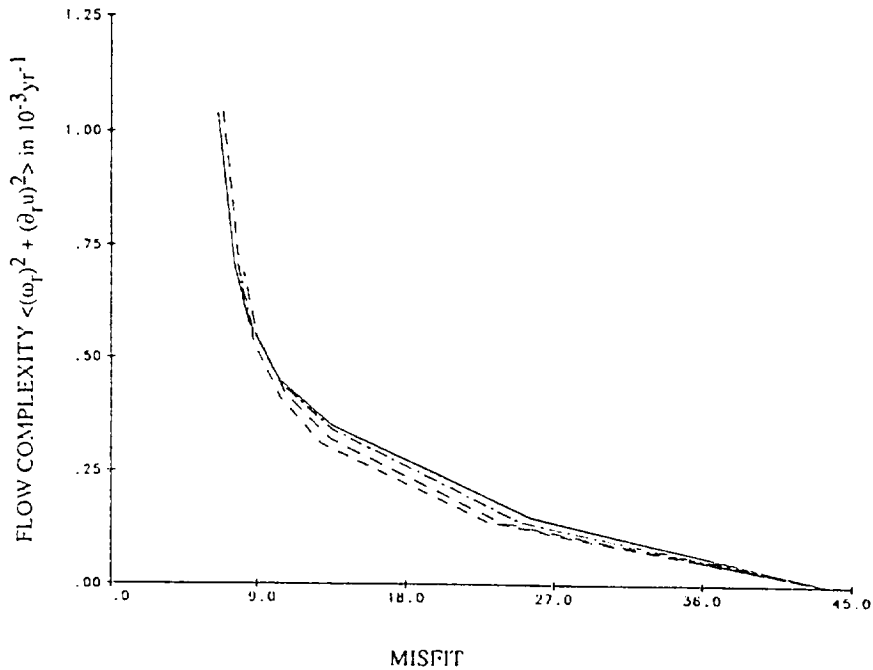


Fig. 2. Trade-off curves showing flow complexity as a function of misfit for 4 conductivity profiles. Flow complexity is the square root of the mean square radial vorticity plus the mean square surface divergence of the fluid motion; misfit is the square root of the square weighted residual per degree of freedom. The solid curve is for profile A (an insulating mantle); the dot-dashed curve adjacent to case A is for profile C; the long-dashed curve adjacent to case C is for profile G; the short-dashed curve adjacent to case G is for profile E.

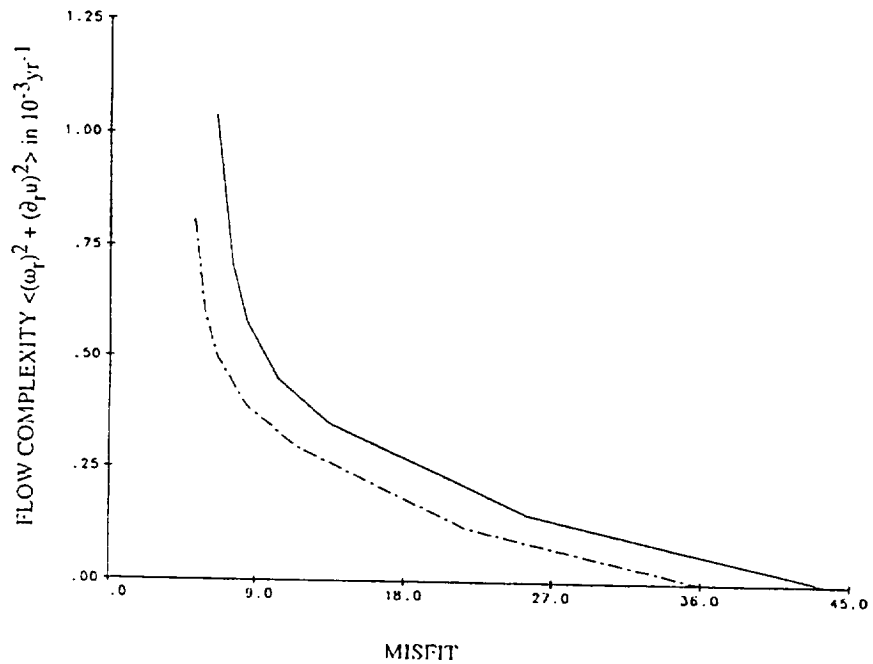


Fig. 3. Trade-off curves showing flow complexity as a function of misfit: solid curve is from the fixed initial geomagnetic condition case with mantle conductivity profile A (insulating mantle; same as solid curve in Fig. 2). Dot-dashed curve is from simultaneous solutions for core field and flow and conductivity profile A. Trade-off curves from simultaneous solutions for core field and flow and conductivity profiles E and G are not shown, but match the dot-dashed curve shown.

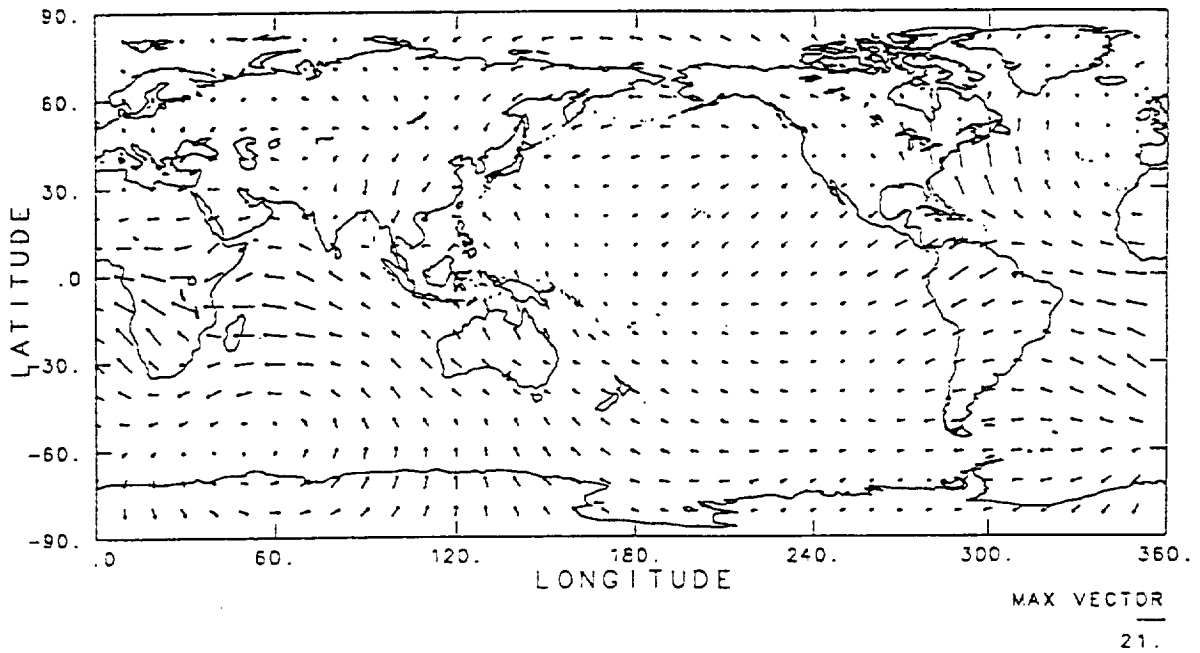
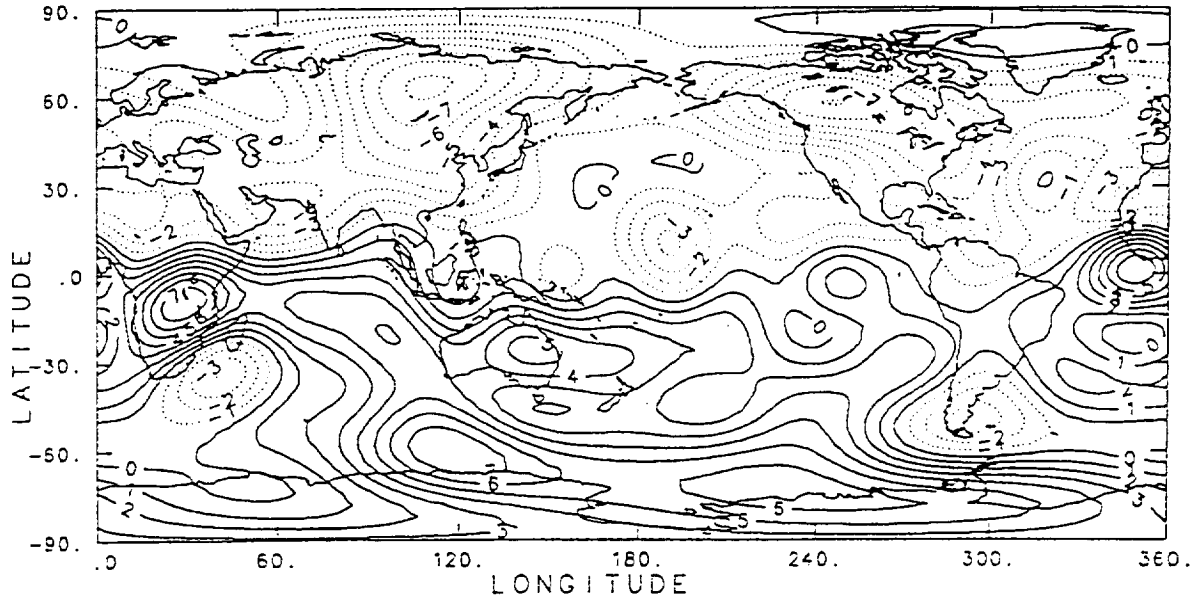


Fig. 4. A sample of simultaneous solutions for core field and frozen-flux flow beneath an electrically conducting mantle corresponding to the top of the dot-dashed curve in Fig. 3, but for mantle conductivity profile E. The upper panel contours the radial magnetic flux density at the CMB at epoch 1965 with a 1 gauss interval. The lower panel shows the accompanying steady surficial core flow; the reference vector corresponds to the maximum speed of 21 km/yr.

steady surficial core flow estimates are themselves insensitive to mantle conductivity—again provided both the initial core field and the steady core surface flow are solved for. Contour maps of the initial core field at epoch 1965, including null-flux contour topology, proved but weakly sensitive to conductivity profile and flow damping.

Figure 4 shows a sample of our simultaneous solutions for core field and steady frozen-flux flow beneath an electrically conducting mantle. The estimate portrayed corresponds to the top of the dot-dashed trade-off curve in Figure 3, but it is for conductivity profile E. The upper panel is a contour map of the radial magnetic flux density at the CMB at epoch 1965 (contour interval is 1 gauss); the features mapped are quite similar to those appearing on other maps of the recent radial field at the CMB (see, e.g., Benton *et al.* [1979], Voorhies [1984], and Benton & Kohl [1986]). The lower panel shows the accompanying steady surficial core flow; it is similar to the flow shown in Fig. 3 of Voorhies [1993]. Although this solution is for conductivity profile E, similar maps could be shown for other conductivity profiles (as well as for the finite effective magnetic Reynolds number characterizing fluid flow near the top of a finite conductivity core).

Taken together, the field and flow shown in Figure 4 account for 98.72% of Δ_T^2 in (8) with $\gamma_p(t_s)$ taken as $g_p(1965)$; they thus account for about 98.72% of the square-weighted secular change signal in the DGRFs. The misfit achieved is 5.17, so we suggest that $(\chi^2/\text{DOF})^{1/2}$ may well exceed 2.5—as expected for so simple an Earth model. The solution is characterized by 193 effectively free parameters: 120 for the initial field and 73 for the core flow. The RMS residual in B_r relative to the 1980 DGRF is 61 nT (about one year worth of SV). At epoch 1965, the RMS value for B_r at the CMB (through degree and order 10) is 3.02 gauss, while the RMS value of predicted $\partial_t B_r$ at the CMB is 3.04×10^3 nT/yr. The flow complexity is $8.11 \times 10^{-3} \text{ yr}^{-1}$; the RMS flow speed is 8.41 km/yr; the RMS downwelling is $5.76 \times 10^{-3} \text{ yr}^{-1}$; and the bulk westward drift underlying the flow is $0.121^\circ/\text{yr}$;

Summary

The effects of laterally homogeneous mantle electrical conductivity have been included in steady, frozen-flux core surface flow estimation along with some refinements in method and weighting. The refined method allows simultaneous solution for both the initial radial geomagnetic field component at the core-mantle boundary (CMB) and the sub-adjacent fluid motion; it also features Gauss' method for solving the nonlinear inverse steady motional induction problem. The tradeoff between spatial complexity of the derived flows and misfit to the weighted Definitive Geomagnetic Reference Field models (DGRFs) has been studied for several mantle conductivity profiles. For simple flow and a fixed initial geomagnetic condition, a fairly high deep-mantle conductivity performs better than either insulating or weakly conducting profiles; however, a thin, very high conductivity layer at the base of the mantle performs almost as well. Simultaneous solution for both initial geomagnetic field and fluid flow reduces the square-weighted residuals per degree of freedom even more than does changing the mantle conductivity profile. Indeed, when both core field and flow are estimated, the performance of the solutions become insensitive to the conductivity profile—as do vector plots of the fluid flow.

Explication of definitive secular change in terms of steady frozen-flux flow beneath a conducting mantle yields no clearly preferred mantle conductivity profile when both core field and flow are estimated; therefore, the results of this study in no way conflict with the finding by McLeod [1992] that observatory annual means are consistent with a nearly insulating mantle surrounding a highly conducting core. Furthermore, our results neither support nor discount the possibility of a thin, very high conductivity layer at the base of the mantle. Indeed, we find that our estimates of steady core surface flow are insensitive to the effects of such a hypothetical layer. Whether such a layer strongly influences estimates of time-dependent core surface flow remains to be seen.

Neither the effects of mantle conductivity nor the simultaneous solution for core field and flow reduced our square-weighted residuals per degree of freedom to unity. Clearly such residuals could easily be explained in terms of time-dependent magnetic flux diffusion near the top of Earth's core. Moreover, there is some chance that additional allowances for the effects of steady magnetic flux diffusion (studied separately by Voorhies [1993]) and of core asphericity could yield a tolerable fit. Nevertheless, our preferred interpretation of the modest misfit to the DGRFs found in this study (and in the study by Voorhies [1993]) is that it provides some evidence for time-dependent core surface flow.

Acknowledgments. Our special thanks to T. Sabaka for providing fresh insights into the inverse steady motional induction problem and covariances for several DGRF models, and to B. Bills for helpful comments on the manuscript. Our thanks to the people of the United States of America who supported this work via their National Aeronautics and Space Administration RTOP 579-31-07.

References

- Achache, J., J.-L. LeMouél, and V. Courtillot, Long-period variations and mantle conductivity: an inversion using Bailey's method, *Geophys. J. R. Astr. Soc.*, *65*, 579-601, 1981.
- Allredge, L. R., Deep mantle conductivity, *J. Geophys. Res.*, *82*, 5427-5431, 1977.
- Allredge, L. R., On predicting changes in the geomagnetic field, *J. Geophys. Res.*, *92*, 6331-6338, 1987.
- Backus, G. E., Kinematics of the secular variation in a perfectly conducting core, *Phil. Trans. Roy. Soc. Lond.*, *A263*, 239-266, 1968.
- Backus, G. E., The electric field produced in the mantle by the dynamo in the core, *Phys. Earth Planet. Inter.*, *28*, 191-214, 1982.
- Backus, G. E., Application of mantle filter theory to the magnetic jerk of 1969, *Geophys. J. R. Astr. Soc.*, *74*, 713-746, 1983.
- Backus, G. E., Poloidal and toroidal fields in geomagnetic field modeling, *Rev. Geophys.*, *24*, 75-109, 1986.
- Backus, G. E., and J.-L. LeMouél, The region on the core-mantle boundary where a geostrophic velocity field can be determined from frozen-flux geomagnetic data, *Geophys. J. R. Astr. Soc.*, *85*, 617-628, 1986.
- Banks, R. J., Geomagnetic variations and the electrical conductivity of the upper mantle, *Geophys. J. R. Astr. Soc.*, *17*, 457-487, 1969.
- Benton, E. R., and M. A. Celaya, The simplest, unsteady surface flow of a frozen-flux core that exactly fits a geomagnetic field model, *Geophys. Res. Lett.*, *18*, 577-580, 1991.
- Benton, E. R., and B. C. Kohl, Geomagnetic main field analysis at the core-mantle boundary: spherical harmonics compared with harmonic splines, *Geophys. Res. Lett.*, *13*, 1533-1536, 1986.
- Benton, E. R., L. A. Muth, and M. Stix, Magnetic contour maps at the core-mantle boundary, *J. Geomag. Geoelectr.*, *31*, 615-626, 1979.
- Benton, E. R., and C. V. Voorhies, Testing recent geomagnetic field models via magnetic flux conservation at the core-mantle boundary, *Phys. Earth Planet. Inter.*, *48*, 350-357, 1987.
- Benton, E. R., and K. A. Whaler, Rapid diffusion of the poloidal geomagnetic field through a weakly conducting mantle: a perturbation solution, *Geophys. J. R. Astr. Soc.*, *75*, 77-100, 1982.
- Bloxham, J., The steady part of the secular variation of the Earth's magnetic field, *J. Geophys. Res.*, *97*, 19,565-19,579, 1992.
- Bloxham, J. and Gubbins, D., Geomagnetic field analysis -IV. Testing the frozen-flux hypothesis, *Geophys. J. R. Astr. Soc.*, *84*, 139-152, 1986.
- Bloxham, J., and A. Jackson, Fluid flow near the surface of Earth's outer core, *Rev. Geophys.*, *29*, 97-120, 1991.
- Bloxham, J., and A. Jackson, Time-dependent mapping of the magnetic field at the core-mantle boundary, *J. Geophys. Res.*, *97*, 19,537-19,563, 1992.
- Booker, J. R., Geomagnetic data and core motions, *Proc. Roy. Soc.*, *A309*, 27-40, 1969.
- Constable, C. G., R. L. Parker, and P. B. Stark, Geomagnetic field models incorporating frozen-flux constraints, *Geophys. J. Int.*, *113*, 419-433, 1993.

- Davis, R. G., and K. A. Whaler, Constant velocity fields at the top of the earth's core from 1915-1975, *Geophys. Astrophys. Fluid Dyn.*, , in press, 1993.
- Eckhardt, D., K. Larnier, and T. Madden, Long-period magnetic fluctuations and mantle electrical conductivity estimates, *J. Geophys. Res.*, 68, 6279-6291, 1963.
- Hide, R., and S. R. C. Malin, On the determination of the size of the Earth's core from observations of the geomagnetic secular variation, *Proc. R. Soc. Lond.*, A374, 15-33, 1981.
- IAGA, Division I Working Group 1, International Geomagnetic Reference Field Revision 1987, *Phys. Earth Planet. Inter.*, 50, 209-213, 1988.
- Jackson, A., J. Bloxham, and D. Gubbins, Time-dependent flow at the core surface and conservation of angular momentum in the coupled core-mantle system, *Geophys. Mono.*, 72, 97-107, 1993.
- Knittle, E., R. Jeanloz, A. C. Mitchell, and W. J. Nellis, Metalization of $\text{Fe}_{0.94}\text{O}$ at elevated pressures and temperatures observed by shock-wave electrical resistivity measurements, *Solid State Comm.*, 59, 513-515, 1986.
- Lahiri, B. N., and A. T. Price, Electromagnetic induction in non-uniform conductors, and the determination of the conductivity of the earth from terrestrial magnetic variations, *Phil. Trans. Roy. Soc.*, A237, p64, 509-540, 1939.
- Langel, R. A., R. H. Estes, and T. J. Sabaka, Uncertainty estimates in geomagnetic field modeling, , *J. Geophys. Res.*, 94, 12,281-12,299, 1989.
- Li, X., and R. Jeanloz, Electrical conductivity of $(\text{Mg,Fe})\text{SiO}_3$ perovskite and a perovskite dominated assemblage at lower mantle conditions, *Geophys. Res. Lett.*, 11, 1075-1078, 1987.
- McDonald, K. L., Penetration of the geomagnetic secular variation through a mantle with variable conductivity, *J. Geophys. Res.*, 62, 117-141, 1957.
- McLeod, M. G., Signals and noise in magnetic observatory annual means: mantle conductivity and jerks, *J. Geophys. Res.*, 97, 17,261-17,290, 1992.
- Peyronneau, J., & J. P. Poirier, Electrical conductivity of the Earth's lower mantle, *Nature*, 342 537-539, 1989.
- Rikitake, T., Global electrical conductivity of the Earth, *Phys. Earth Planet. Inter.*, 7, 245-250, 1973.
- Roberts, P. H., and S. Scott, On analysis of secular variation 1. A hydromagnetic constraint, *J. Geomag. Geoelectr.*, 17, 137-151, 1965.
- Sabaka, T. J., R. T. Baldwin, C. V. Voorhies, and R. A. Langel, Simultaneous estimation of core flow and magnetic field initial condition from direct magnetic field measurements, *Trans. Am Geophys. Un.*, 73 (supplement), 98, 1992.
- Stacey, F. D., *Physics of the Earth*, John Wiley & Sons, New York, 413 pp., 1977.
- Voorhies, C. V., Magnetic Location of Earth's Core-Mantle Boundary and Estimates of the Adjacent Fluid Motion, Ph.D. thesis, Univ. of Colo., Boulder, 348 pp., 1984.
- Voorhies, C. V., Steady flows at the top of Earth's core derived from geomagnetic field models, *J. Geophys. Res.*, 91, 12,444-12,466, 1986a.
- Voorhies, C. V., Steady surficial core motions: an alternate method, *Geophys. Res. Lett.*, 13, 1537-1540, 1986b.
- Voorhies, C. V., The time-varying geomagnetic field, *Rev. Geophys.*, 25, 929-938, 1987.
- Voorhies, C. V., Coupling and inviscid core to an electrically insulating mantle, *J. Geomag. Geoelectr.*, 131-156, 1991.
- Voorhies, C. V., Steady induction effects in geomagnetism Part IA: steady motional induction of geomagnetic chaos, *NASA Technical Paper 3272, Part IA*, 28 pp., 1992.
- Voorhies, C. V., Geomagnetic estimates of steady surficial core flow and flux diffusion: unexpected geodynamo experiments, *Geophys. Mono.*, 72, 113-125, 1993.
- Voorhies, C. V., and G. E. Backus, Steady flows at the top of the core from geomagnetic field models: the steady motions theorem, *Geophys. Astrophys. Fluid Dyn.*, 32, , 163-173, 1985.
- Voorhies, C. V., and E. R. Benton, Pole strength of the Earth from MAGSAT and magnetic determination of the core radius, *Geophys. Res. Lett.*, 9, 258-261, 1982.
- Whaler, K. A., Properties of steady flows at the core-mantle boundary in the frozen-flux approximation, *Phys. Earth Planet. Inter.*, 68, 144-155, 1991.

REPORT DOCUMENTATION PAGE

Form Approved
OMB No. 0704-0188

Public reporting burden for this collection of information is estimated to average 1 hour per response, including the time for reviewing instructions, searching existing data sources, gathering and maintaining the data needed, and completing and reviewing the collection of information. Send comments regarding this burden estimate or any other aspect of this collection of information, including suggestions for reducing this burden, to Washington Headquarters Services, Directorate for Information Operations and Reports, 1215 Jefferson Davis Highway, Suite 1204, Arlington, VA 22202-4302, and to the Office of Management and Budget, Paperwork Reduction Project (0704-0188), Washington, DC 20503.

1. AGENCY USE ONLY (Leave blank)	2. REPORT DATE September 1993	3. REPORT TYPE AND DATES COVERED Technical Paper	
4. TITLE AND SUBTITLE Simultaneous Solution for Core Magnetic Field and Fluid Flow Beneath an Electrically Conducting Mantle		5. FUNDING NUMBERS Code 921	
6. AUTHOR(S) Coerte V. Voorhies and Masahiro Nishihama			
7. PERFORMING ORGANIZATION NAME(S) AND ADDRESS(ES) Goddard Space Flight Center Greenbelt, Maryland 20771		8. PERFORMING ORGANIZATION REPORT NUMBER 93E02367	
9. SPONSORING/MONITORING AGENCY NAME(S) AND ADDRESS(ES) National Aeronautics and Space Administration Washington, D.C. 20546-0001		10. SPONSORING/MONITORING AGENCY REPORT NUMBER NASA TM-4536	
11. SUPPLEMENTARY NOTES Masahiro Nishihama: Hughes STX Corporation, Lanham, Maryland.			
12a. DISTRIBUTION/AVAILABILITY STATEMENT Unclassified-Unlimited Subject Category 46 Report available from the NASA Center for AeroSpace Information, 800 Elkridge Landing Road, Linthicum Heights, MD 21090; (301) 621-0390.		12b. DISTRIBUTION CODE	
13. ABSTRACT (Maximum 200 words) The effects of laterally homogeneous mantle electrical conductivity have been included in steady, frozen-flux core surface flow estimation along with refinements in method and weighting. The refined method allows simultaneous solution for both the initial radial geomagnetic field component at the core-mantle boundary (CMB) and the sub-adjacent fluid motion; it also features Gauss' method for solving the non-linear inverse problem associated with steady motional induction. The tradeoff between spatial complexity of the derived flows and misfit to the weighted Definitive Geomagnetic Reference Field models (DGRFs) is studied for various mantle conductivity profiles. For simple flow and a fixed initial geomagnetic condition, a fairly high deep-mantle conductivity performs better than either insulating or weakly conducting profiles; however, a thin, very high conductivity layer at the base of the mantle performs almost as well. Simultaneous solution for both initial geomagnetic field and flow reduces the misfit per degree of freedom even more than does changing the mantle conductivity profile. Moreover, when both core field and flow are estimated, the performance of the solutions and the derived flows become insensitive to the conductivity profile.			
14. SUBJECT TERMS Geophysics, Geomagnetism, Earth's Core, Core Field, Core Fluid Motion		15. NUMBER OF PAGES 14	
		16. PRICE CODE	
17. SECURITY CLASSIFICATION OF REPORT Unclassified	18. SECURITY CLASSIFICATION OF THIS PAGE Unclassified	19. SECURITY CLASSIFICATION OF ABSTRACT Unclassified	20. LIMITATION OF ABSTRACT Unlimited